International Journal of Heat and Fluid Flow 29 (2008) 1369–1379

Contents lists available at ScienceDirect

International Journal of Heat and Fluid Flow

journal homepage: www.elsevier.com/locate/ijhff

Studies on the starting transient of a straight cylindrical supersonic exhaust diffuser: Effects of diffuser length and pre-evacuation state

Byung Hoon Park [a,1], Ji Hyung Lee [a,1], Woongsup Yoon [b,*]

[a] Propulsion and Environmental Thermo-Fluids Laboratory, A582, School of Mechanical Engineering, Yonsei University 134, Shinchon-dong, Seodaemun-gu, Seoul 120-749, South Korea

[b] Propulsion and Environmental Thermo-Fluids Laboratory, A377, School of Mechanical Engineering, Yonsei University 134, Shinchon-dong, Seodaemun-gu, Seoul 120-749, South Korea

ARTICLE INFO

Article history:
Received 7 August 2007
Received in revised form 7 April 2008
Accepted 8 April 2008
Available online 3 June 2008

Keywords:
Supersonic exhaust diffuser (SED)
High altitude test (HAT)
Starting transient
Short diffuser
Diffuser mode-transition

ABSTRACT

Effects of essential performance parameters on the starting transient of a straight cylindrical supersonic exhaust diffuser (SED) are numerically investigated. Diffuser starting and evacuation transients are examined in terms of SED lengths and pre-evacuation configuration. Preconditioned Favre-averaged Navier–Stokes equations incorporated with a low Reynolds number turbulence model and Sakar's method to treat turbulence compressibility is solved for strongly turbulent all-Mach diffuser flows. The numerical method is properly validated with the measurements with accuracy. Characteristic locus of diffuser-starting and diffuser-unstarting modes is constructed for the diffusers of three different lengths (L/D = 2, 5, and 20). Flow evolutions visualized in diffuser mode-transition regimes manifest a threshold L/D over which the SED starting transient is unique. An occurrence of plume blowback into the vacuum chamber due to lower initial pressure ($P_{C,INIT}/P_A$ = 0.0027) expedites expansion of nozzle exhaust and diffuser choking, and causes faster chamber evacuation than the atmospheric starting.

1. Introduction

By all means, a rocket engine designed to operate in the upper atmosphere or space of higher vacuum state requires a pre-flight test in order to verify its static and dynamic performances and environmental suitability at low pressures. This high-altitude rocket engine is typically equipped with a high-expansion-ratio nozzle for producing maximum momentum thrust available at higher vacuum state. And the test data measured at sea-level pressure is significantly underestimated from its expected values at high altitudes. Secondary flow phenomena such as reversing flows and corresponding flow separation at diverging section of the supersonic nozzle are induced by unbalanced nozzle-exit and ambient pressures due to the higher nozzle expansion ratio optimized for low-pressure functioning. Unacceptably poor verification is commonplace, and thus the use of high altitude test (HAT) facilities is prerequisite to the ground verification of the high altitude engines including thrust level, thermal compatibility, vacuum ignition, and endurance capabilities of all the engine components. By lowering the back pressure in the interval of engine operation, the altitude simulation can meet the nozzle full-flow condition (Massier and Roschke, 1960; Schäfer and Zimmermann, 2004).

HAT facilities of sufficient capacity to accommodate full-scale engine testing are bulky and expensive. Besides, an ejector system equipped with a second throat and secondary gas stream raises the complexity in designing the HAT. Thus, as a viable substitute for the ejector system, a straight cylindrical supersonic exhaust diffuser (SED) with no secondary gas injection has been extensively used owing to its simplicity and a small outlay. Each operating mode of the straight cylindrical SED, the diffuser-unstarting and the diffuser-starting modes, has its own proportional share in their applications. On one hand, the diffuser-unstarting mode is often fit for a commercial purpose, such as refrigeration, air-conditioning, power generation and gas vapor recovery (Sun and Eames, 1995). On the other hand, use of the diffuser-starting mode is mostly confined to an aerospace application.

A number of studies on HAT have generally focused on examining the steady evacuation quality in terms of essential operational and geometrical parameters of the diffuser (Massier and Roschke, 1960; Taylor, 1969). Comprehensive experimental studies on a variety of diffuser configurations revealed that the diffuser (evacuation) performance is well characterized by starting and operating nozzle pressures. Annamalai et al. (1998, 2000) conducted a series of full-scale motor tests using both non-reactive nitrogen gas and hot rocket exhaust as working fluids. A brief summary on scaling criteria was also addressed with regard to a correction factor (K-factor) in order to take the effects of diffuser length into account. Paralleled with these experimental efforts, computer methods based on computational fluid dynamics (CFD) were also practiced

* Corresponding author. Tel.: +82 2 2123 4812.
E-mail addresses: engineer@yonsei.ac.kr (B.H. Park), im_ljh@yonsei.ac.kr (J.H. Lee), wsyoon@yonsei.ac.kr (W. Yoon).
[1] Tel.: +82 2 2123 4812.

0142-727X/$ - see front matter © 2008 Elsevier Inc. All rights reserved.
doi:10.1016/j.ijheatfluidflow.2008.04.006

Notation

A_D	cross-sectional area of supersonic diffuser
$A_{D,MAX}$	maximum cross-sectional area for diffuser starting
A_N	cross-sectional area of nozzle exit
A_T	cross-sectional area of nozzle throat
D	diameter of supersonic diffuser
D_E	diameter of diffuser exit (=$2R_E$)
D_T	diameter of nozzle throat
L	length of supersonic diffuser
L_S	length of subsonic diffuser
L/D	length-to-diameter ratio of diffuser
$(L/D)_{OPT}$	optimum length-to-diameter ratio
M_i	Mach number at diffuser inlet
P_A	ambient pressure, 1 atm
P_{AVG}	area-averaged pressure
P_C	static pressure in vacuum chamber
$P_{C,INIT}$	initial cell pressure
P_E	static pressure at diffuser exit
P_i	static pressure at diffuser inlet
P_0	total pressure at nozzle inlet
$P_{0,OPT}$	optimum starting pressure
$P_{0,STD}$	total pressure at nozzle inlet at steady operation
X_D	axial location of supersonic diffuser inlet
X_F	far-field distance from diffuser exit in axial direction
X_N	axial location of nozzle exit
Y_F	far-field distance from diffuser centerline in radial direction
Greek	
k	specific heat ratio

not only for cost-effective performance prediction but also for visualization of complex diffuser flows such as internal shock wave structures (Sankaran et al., 2002; Desevaux and Lanzetta, 2004; Bartosiewicz et al., 2005). With regard to the steady evacuation performance of a second-throat exhaust diffuser (STED), Sankaran et al. (2002) conducted numerical experiments and showed that the performance of the STED can be correctly predicted by the flow solvers using RANS method. Desevaux and Lanzetta (2004) attempted similar numerical experiments and compared static pressures along the centerline of a zero-secondary flow ejector and non-dimensional pseudo-shock lengths in diffuser-unstarting mode. As a part of effort to improve an applicability of numerical methods with accuracy, Bartosiewicz et al. (2005) conducted comprehensive numerical study and examined six turbulence models of k–ε, realizable k–ε, RNG-k–ε, RSM, and two k–ω aiming at determining more suitable turbulence model in the case of supersonic ejectors for refrigeration application. Obviously, the CFD deserves to be an alternative as an effective diagnostic tool for analysis, design, and performance optimization of the HAT.

Interestingly, researches to get better understandings and thus to deal with starting and terminating transients of the diffuser operation are very few. Since the starting transient rarely alters the steady functions of the diffuser in HAT, such indifferences are assented while an emphasis is laid on the steady performance only. However, experimental results conducted in the present study evidence that changes in the starting transient caused by different test condition such as atmospheric or low starting pressure may lead to a vastly altered flow profile. Since an upper-stage rocket motor functions at lower or near zero pressures, the vacuum ignition test is indispensable and thus must be exercised as a part of altitude simulation. Prior to the motor ignition, a test-cell (vacuum chamber in Fig. 1) of SED which lacks in steam ejector system must be pre-evacuated by an external vacuuming device. Prior to uncovering of diffuser exit, the nozzle exhaust evolves while it forms very complicated flows at an early stage of the starting transient, and rapid cell-pressurization shortens initiation period for charging the diffuser cell and reaching the steady operation. Strong transient effects also occur during termination stage at motor tail-off. With no presence of secondary flow injected from steam ejector system, the termination of diffuser function causes evacuated test-cell suddenly exposed to the atmosphere. Thus, plume blowback at diffuser breakdown always occurs during the motor tail-off period in the HAT. Soaking-back of heat due to the plume shrinking may cause overheating or even burning of the system hardware. Anomalies in the process of data recording and acquisition possibly happen. To avoid such strong transient stiffness,

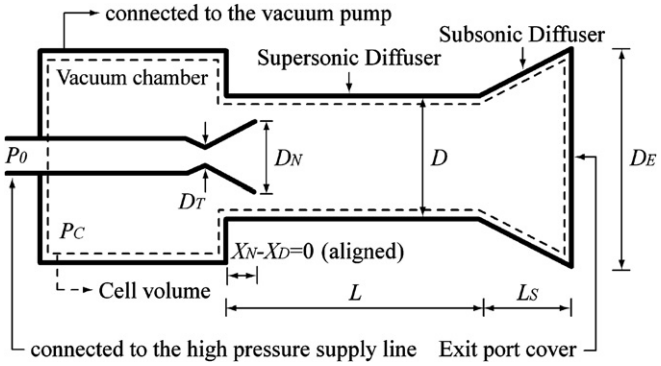

Fig. 1. Installation schematic of an altitude simulator equipped with a straight cylindrical SED.

plume blowback is frequently alleviated by water-spray or nitrogen-purging through internal flow passage. Clear understanding of this tail-off phenomenon due to direct contact of evolving nozzle gases to the external nozzle surface is essential to compatibility design of the HAT (NASA Lewis Research Center, 1971; Stephens et al., 1991).

Other transient effects are originated from the diffuser mode-transition regime and the geometric parameters. As will be described later, the pressure records in vacuum chamber (P_C) during starting transients in diffuser mode-transition regime are not the same with those in diffuser-unstarting and diffuser-starting modes. Here, the diffuser mode-transition regime is defined as an interval between diffuser-unstarting and diffuser-starting mode, and P_0 in this regime is slightly higher than an optimum starting pressure ($P_{0,OPT}$). Retardation of the supersonic jet impingement onto diffuser inlet wall is a possible cause for this peculiarity. The geometrical parameters, such as A_D/A_T, A_D/A_N, and L/D, also affect the evolution of the diffuser flows and alter the startability of the SED.

Detailed information on aforementioned transient phenomena relevant to SED operation is essential to the safety and compatibility design of HAT. These critical issues, however, have not been carefully touched or even excluded from the HAT design. It is mainly due to the facts that experimental methods is hardly able to resolve complex internal flows in the SED, and thus rigorous dynamics design was not amenable. Hence, the present study extends author's previous work (Park et al., 2008) on the transient fluid dynamics in the SED. With reference to previous investigation

on the starting and terminating diffuser dynamics, the starting transients of straight cylindrical SED with different diffuser lengths and different initial evacuation level are investigated. A preconditioned Favre-averaged Navier–Stokes in-house solver with a low-Reynolds number k–ε turbulence model solves diffuser flows. Sakar's model incorporated into the turbulence model treats turbulence compressibility effect. Parametric investigations of the SED transients due to changes in the *L/D* and the evacuation levels are made and detailed descriptions on the transient diffuser flows are addressed.

2. HAT starting with a straight cylindrical SED

An altitude simulator equipped with a constant-area duct type diffuser is typically constructed with three major parts: (1) test-cell (vacuum chamber); (2) nozzle; (3) diffuser (Fig. 1). According to its definition, the diffuser decelerates nozzle exhaust plume, but this function is performed only when the chamber stagnation pressure at steady operation $P_{0,STD}$ is higher than the critical pressure which is a minimum $P_{0,STD}$ for the diffuser choking. This minimum diffuser choking pressure is equivalent to an optimum starting pressure $P_{0,OPT}$ (Fig. 2). The diffuser is choked when expanding nozzle exhaust impinges on diffuser inlet wall and then isolates the vacuum chamber from the diffuser downstream after the impingement point. Then the states of the diffuser upstream are independent of downstream condition and the evacuation quality in the vacuum chamber is a function of the flow properties of blocking nozzle exhaust only.

Immediately after motor ignition, exhaust gas starts to expand from the nozzle exit and entrains the gas in the vacuum chamber due to (1) the static pressure lower than that initial cell pressure, and (2) the momentum transfer by high-speed nozzle exhaust. After successive suction of initial cell gas and chamber evacuation during a starting transient, the test-cell (vacuum chamber) reaches its higher vacuum state and provides a low pressure environment in the vicinity of nozzle exit while it mimics a high-altitude space.

To secure solid starting of a diffuser, the diffuser geometry must be suitably chosen in the range that it fulfills the specific motor requirement. The geometrical parameters relevant to exhaust-gas impingement and chamber isolation such as A_D/A_T, A_D/A_N, and *L/D* are compulsory items to be considered. For instance, normal shock theory yields thermodynamic area-pressure ratio relations in terms of Mach number (Eq. (1)), and provides rough prediction of $P_{0,OPT}$ in terms of A_D/A_T (Fig. 3). For a given P_0, this relation calculates $A_{D,MAX}/A_T$ required for starting a diffuser. Since a diffuser

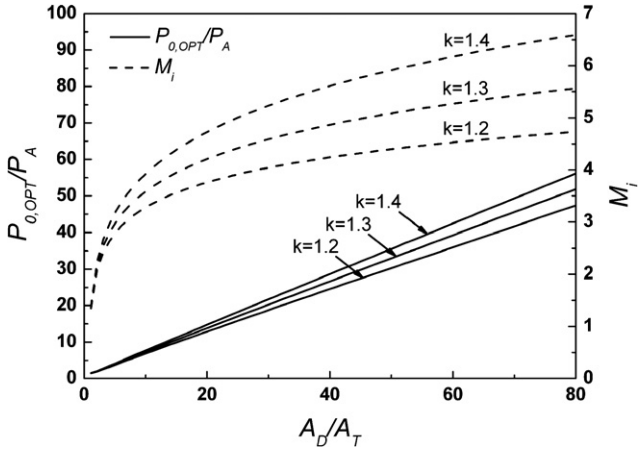

Fig. 3. Theoretical optimum starting pressure ($P_{0,OPT}$) and Mach number at diffuser inlet (M_i) as a function of diffuser-to-throat area ratio (Eq. (1)).

with A_D greater than $A_{D,MAX}$ is not starting, the area ratio must be lower than $A_{D,MAX}/A_T$ at P_0.

$$A_D/A_T = \frac{1}{M_i}\left[\frac{2}{k+1}\left(1+\frac{k-1}{2}M_i^2\right)\right]^{\frac{k+1}{2(k-1)}}$$
$$P_{0,OPT}/P_A = \left[1+\frac{k-1}{2}M_i^2\right]^{\frac{k}{k-1}} \Big/ \left[\frac{2k}{k+1}M_i^2 - \frac{k-1}{k+1}\right] \quad (1)$$

If the diffuser–nozzle area ratio (A_D/A_N) is not much greater than unity, test-cell decompression during a starting transient progresses is retarded with gradual decrease in P_C. It is because that the mass entrainment rate from the test-cell into the diffuser is proportional to $A_N(A_D/A_N - 1)$ where A_D and A_N are the cross-sectional areas of the diffuser and the nozzle exit, respectively (Fig. 1). Here, A_D/A_N directly estimates the clearance between the nozzle exit and the inner wall of the diffuser. Fig. 4 compares two different evacuation histories (normalized chamber pressure) after the motor initiation. Two diffusers of case 1A with A_D/A_N = 1.15 and case 1 with A_D/A_N = 5 are examined with same charging sequence of P_0/P_A (Table 1). Due to relatively smaller A_D/A_N of 1.15, the case 1A exhibits longer relaxation time (interval reaching steady operation) than that of the case 1. Thrust distortion during terminating transient is anticipated for test case 1A of smaller A_D/A_N since the break down process occurring in a smaller A_D/A_N diffuser is more progressive with a

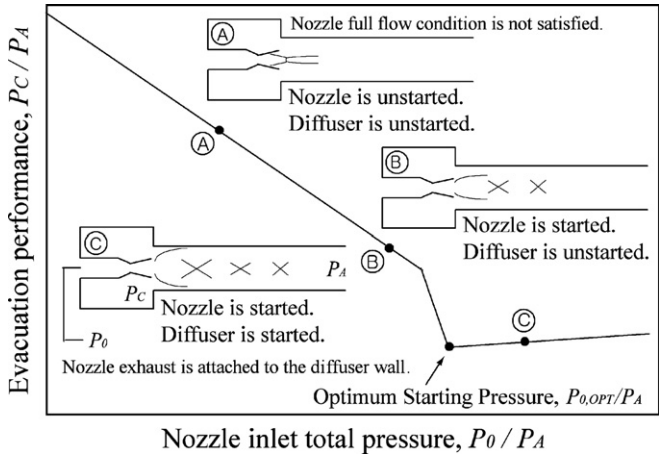

Fig. 2. Illustration of operating sequence and locus for diffuser starting ($P_{0,STD} < P_{0,OPT}$, unstarting; $P_{0,STD} > P_{0,OPT}$, starting).

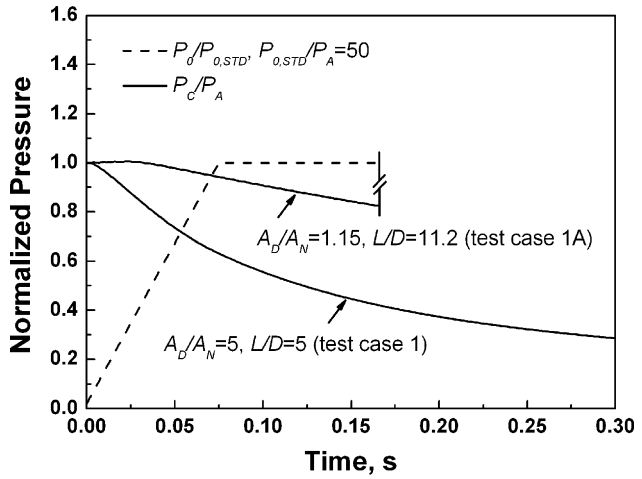

Fig. 4. Effects of diffuser–nozzle area ratio (A_D/A_N) on the evacuation transient (P_C).

Table 1
Geometrical and operational parameters used for HAT simulation

Parameters	Test case 1[a] (without pre-evacuation)	Test case 2 (with pre-evacuation)
Nozzle inlet total pressure, $P_{0,STD}/P_A$	5–50[b]	45.9
Diffuser length-to-diameter ratio, L/D[c]	2.0, 5.0, 20.0	5.0
Nozzle expansion ratio, A_N/A_T	5.68	5.68
Diffuser cross-sectional area ratio, A_D/A_T	28.4	28.4
Initial cell pressure, $P_{C,INIT}/P_A$	1.0	0.0027
Key geometrical factors	L/D and $P_{0,STD}/P_A$	Low $P_{C,INIT}/P_A$
Time-accurate scheme	Steady and unsteady	Unsteady only
Measurements	Real-time pressure records[d]	Real-time pressure records

[a] Test case 1A shown in Fig. 4 was added in order to compare the effect of the diffuser–nozzle area ratio (A_D/A_N) on the evacuation quality in diffuser starting transient.
[b] Two diffuser characteristic curves with L/D of 2 and 5 are made in this range.
[c] Diffuser length L is not inclusive of subsonic diffuser length L_S ($L_S = 1.56D$).
[d] Test cases with L/D of 5 was measured. Other cases were calculated only.

back flow slowly running against the diffuser flows. Thus, even after shutting-down of the tested motor, the pressure is slowly recovering in the test-cell and the motor thrust may be over-estimated by the gas pressure left in the cell volume.

Theoretical formulae for the functional relationship between the diffuser performance and the geometrical and/or operational parameters are not available with an exception of area-pressure ratio relation shown in Eq. (1) for the case of sufficiently long diffuser. Multi-dimensional phenomena and closely coupled participating physics cause such mathematical difficulties, and only the qualitative understandings can be obtained from the theoretical methods. In the present study, two most important factors of diffuser length (L/D) and pre-evacuation state ($P_{C,INIT}$) are numerically examined in order to investigate their effects on evolving diffuser flows in starting transients and global performance of SED.

3. Experimental setup and test matrix

Fig. 5 shows side and plane schematic of a small-scale altitude simulator. Test stand is installed with a vacuum chamber which is connected to the left end of the diffuser. A constant-area duct-type diffuser is assembled next to the nozzle exit with its longitudinal axis aligned with that of the nozzle. Keeping the diffuser exit capped with an exit port cover, a mechanical vacuum pump decompresses the cell volume (a volume inside the dotted line in Fig. 1).

After nozzle inlet pressure is regulated to a target value (P_0), a quick opening value connected to the paralleled high-pressure nitrogen tanks is switched on, and cold nitrogen gas flows into the test nozzle. Immediately after discharging the nozzle exhaust (nitrogen gas) into the diffuser, the supersonic jet from the nozzle exit starts to entrain the gas in the test-cell owing to the (1) pressure difference between the test-cell and diffuser inlet and (2) momentum transfer by the high-speed nozzle exhaust. After successive suction of the chamber gas during the starting transient, the chamber pressure arrives at its highly evacuated steady state and provides a low pressure environment on the periphery of the nozzle exit.

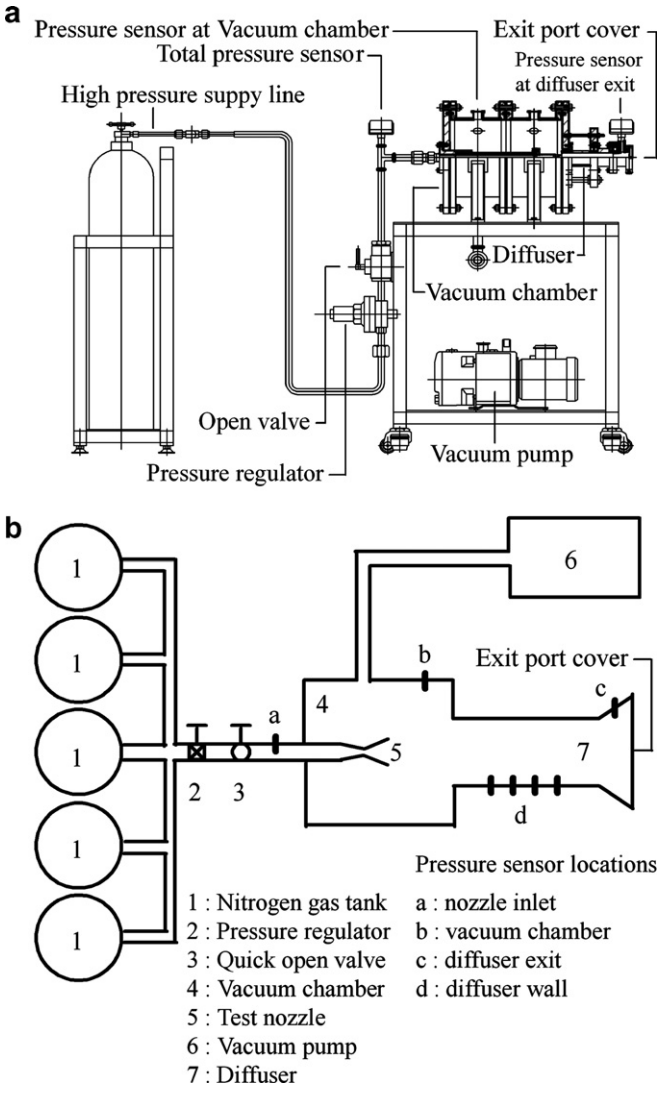

Fig. 5. Schematic of small-scale HAT simulator with straight cylindrical SED.

Instrumentation of pressure sensors is marked on a floor plane of SED simulator shown in Fig. 5b. Two wall-mounted sensors at nozzle inlet (location a) and vacuum chamber (location b) record the static pressures during the starting and terminating transients. Pressure sensors installed spirally around the periphery of the acrylic diffuser (location d) measure the wall static pressures. These sensors are installed exterior of the diffuser pipe and connected to small holes drilled normal to the inner surface of the diffuser. A high-frequency dynamic sensor located near diffuser exit (location c) records fluctuating pressures of secondary flows induced by a separation of diffuser flow and an occurrence of recirculating flow due to diffuser–exterior flow interactions. Park et al. (2008) showed that an incompressible k–ε turbulence scheme implemented with Sakar's turbulence compressibility model correctly depicts complex flow formation in this downstream flow regime.

Essential geometrical and operational test parameters are summarized in Table 1. In case 1, the test cell is not pre-evacuated, and initial chamber pressure $P_{C,INIT}$ is atmospheric due to direct exposure of the cell volume to the atmosphere. Three different length-to-diameter ratios (L/D) are examined to investigate their influences on the evacuation performance of the SED steady operation and associated flow evolutions during the starting transients. Previous study on the steady evacuation performance with several

straight cylindrical diffusers by Annamalai et al. (2000) yielded an optimum L/D of 4.86 when A_D/A_T is 33. The present study set a reference L/D as 5 and examines a shorter ($L/D = 2$) and longer diffusers ($L/D = 20$) with a diffuser-to-nozzle throat area ratio (A_D/A_T) fixed at 28.4. In addition, aiming at determining the locus of optimum starting pressure $P_{0,OPT}$, $P_{0,STD}/P_A$ is varied in the range from 5 to 50 with L/D from 2 to 5. In this case, pressures recorded in the vacuum chamber show a simple exponential decay from its initial state ($P_{0,STD}/P_A = 50$) (Fig. 6a). As time elapses, it gradually arrives at its converged value and the pressure in the vacuum chamber is balanced to the nozzle exhaust pressure.

In case 2, to an end of simulating real situation experienced by an upper-stage rocket motor ignited at low pressure, a mechanical vacuum pump decompresses the cell volume before switching on the diffuser operation. Initial cell pressure ($P_{C,INIT}/P_A$) of 0.0027 is chosen to mimic an upper atmospheric pressure. Once the pressure at nozzle inlet is set to a target value, a quick open value connected to the paralleled high-pressure nitrogen tanks is actuated, and cold nitrogen gas is supplied into the test nozzle. As the pressure exerting on the inner surface of the exit-cover rapidly increases and exceeds the atmospheric pressure, the exit-cover is lifted away and the nitrogen gas inside of the cell volume is discharged out of the diffuser exit. Since the diffuser performance at steady operation does not depend on the initial state, only an unsteady calculation is made for the case 2. With pre-evacuation, the pressure evolution in the vacuum chamber is distinctly different from that in case 1 (Fig. 6b). Compared to Fig. 6a and b shows P_C rapidly settling down to a balanced value (vacuum pressure) followed by a sudden jump immediately after the valve opening.

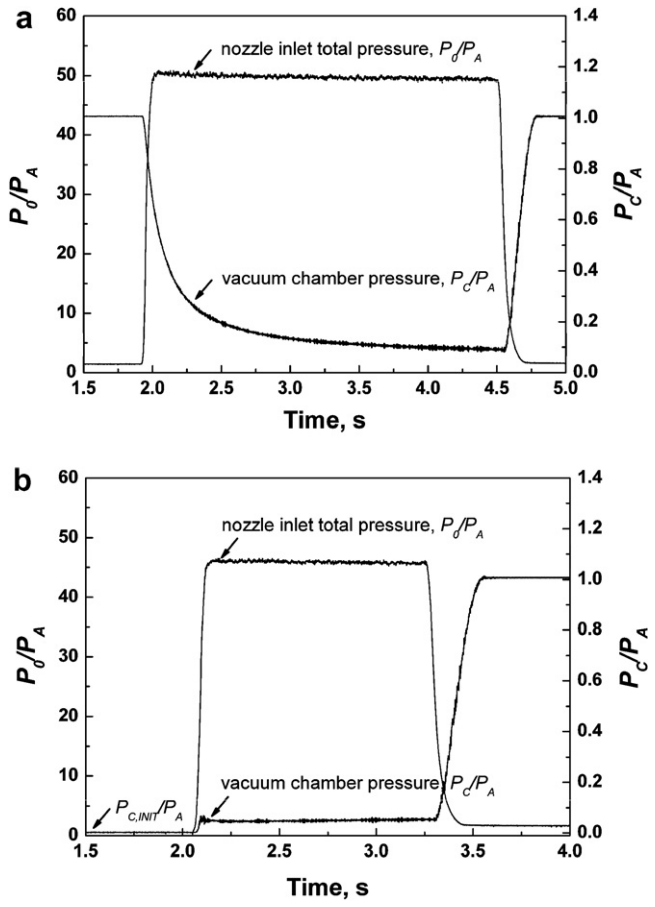

Fig. 6. Total and vacuum chamber pressures at nozzle inlet (a) atmospheric starting (case 1) and (b) starting with pre-evacuation (case 2) with $L/D = 5$.

4. Numerical strategy and solution procedure

4.1. Numerical strategy

Time-dependent strongly conservative axisymmetric Navier–Stokes equations in curvilinear coordinates are solved for complex diffuser flows. To accelerate the convergence rate selectively at any Mach numbers, a local preconditioning method rescales the system eigenvalues (Venkateswaran et al., 2003). Governing flow equations are discretized by cell-vertex finite volume method. A preconditioned flux difference scheme (FDS) is adopted to enhance higher-order spatial accuracy (Hsieh and Yang, 1997). Resultant algebraic equations are solved by LU factorization method using 32-processor parallel cluster. A low Reynolds number k–ε turbulence model (Yang and Shih, 1993) resolves strong turbulence and, as a simple remedy against the innate defect due to turbulence compressibility which is locally important in the SED downstream mixing layer, Sakar's model is incorporated (Shyy and Krishnamurty, 1997). Detailed explanations for the numerical method adopted in the study are described in our previous work (Park et al., 2008)

4.2. Solution procedure

Table 2 summarizes assumptions and simplifications employed for tailoring the problem to an appropriate computational configuration. Included are SED geometry, working fluid, material properties, thermal boundary condition, nozzle inlet total conditions, phase transition, and far-field distance. Since the tested SED is operated by concentric nozzle flow, an overall configuration of the diffuser flows is axisymmetric. This dimensional simplicity brings the simulation with ease of computation. Only one exception is the vacuum chamber clamped by bolted flanges (Fig. 5a). To an end of taking geometrical advantage, however, an inner shape of the vacuum chamber is slightly modified while maintaining the net volume unchanged, so that numerical relaxation time (interval to steady operation) in the starting transient could be the same with the measurement. This simplification is practically acceptable because, in case 1, the vacuum chamber serves as a low pressure reservoir only, and thus influences by slow flows occurring inside the vacuum chamber is minimal and of no practical interest. However, inflowing of the nozzle exhaust into the vacuum chamber in case 2 is an essential route reaching a starting-mode. Supersonic region prevails inside the vacuum chamber before the diffuser-cell is pressurized and the exit-cover capped on diffuser exit is lifted away. Therefore, the computational domain inside the vacuum chamber of the case 2 is slightly modified from that of case 1, and includes an additional block of mesh for a protruded rim of cylindrical flange (Fig. 15).

Since an initial transient of diffuser operation is by and large altered by initial configurations such as state of evacuation and starting sequence, a time-accurate description of the starting dynamics is prerequisite. To this end, the pressurization history at nozzle inlet is measured and interpolated to yield a functional expression of starting sequence. Resultant approximate pressurization curve provides instant total pressure at the nozzle inlet (Fig. 8).

Fig. 9 shows a predicted P_{AVG}, a space-averaged pressure exerting on inner surface of exit-cover, which is obtained from an approximate pressurization curve in Fig. 8b. Once this end-pressure exceeds the atmospheric pressure, the exit-cover is numerically removed (Eq. (2)). This simple scenario of mechanical cover-opening mimics the real situation fairly well, and was successfully adopted for the present calculation strategy with validation. Prior to the removal of the exit-cover, internal flow-field in the cell volume is calculated in advance. After the exit-cover is

Table 2
Geometrical and operational parameters for the tested SED

System configuration	Axisymmetric
Working fluid	Dry nitrogen gas (N_2)
Material properties	Constant transport properties and calorically perfect gas
Thermal boundary condition	Adiabatic wall boundary condition
Nozzle inlet total pressure	Approximated from the measured data (Fig. 8)
Nozzle inlet total temperature	288 K
Phase transition	Not considered
Far-field distance	$X_F/D = 60$, $Y_F/D = 30$

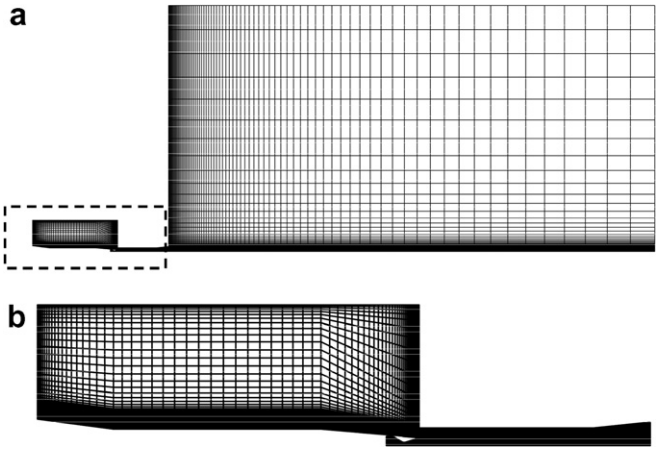

Fig. 7. A structured grid for computation (far-field extended downstream up to $X_F/D = 60$ and $Y_F/D = 30$).

removed, the computational domain is extended to the far-field up to axial and radial distances of $X_F/D = 60$ and $Y_F/D = 30$, respectively (Fig. 7a).

$$P_{AVG}(t) = \frac{1}{\pi R_E^2}\int_{r=0}^{r=R_E} P(t)\,dA \geqslant P_A \tag{2}$$

Flow dynamics in a long diffuser is not hysterical and the minimum starting pressure of SED is regarded as the minimum operating pressure (Massier and Roschke, 1960; Taylor, 1969). In case of a short diffuser, however, diffuser hysteresis is readily observed as demonstrated experimentally by Annamalai et al. (2000). With the presence of hysteresis, which is more plausible for the short diffuser with relatively higher initial pressures, visualization of steady flow cannot be simply made by capturing instant picture of the flow-field since the steady flow might not be unique in time. For the long diffuser, the quasi-steady calculation method is available for flow visualization by following the procedure: (1) unsteady calculation with the nozzle inlet total pressure at the steady operation yields a converged steady solution. (2) This steady solution can be repeatedly used as an initial condition for other steady calculations of different state. In this manner, steady solutions at any $P_{0,STD}$ are readily obtained with CPU economy. But, this method is no longer applicable for the short diffuser calculation in which the occurrence of hysteresis is anticipated. So that use of incorrect initial flow data is avoided, the calculation is made in an unsteady manner.

5. Results and discussion

A diffuser installed in HAT for a ground test of a full-scale rocket motor is exposed to hot gas exhaust. To ensure thermal compatibility from the excessive heat flux so that fatal diffuser burning is

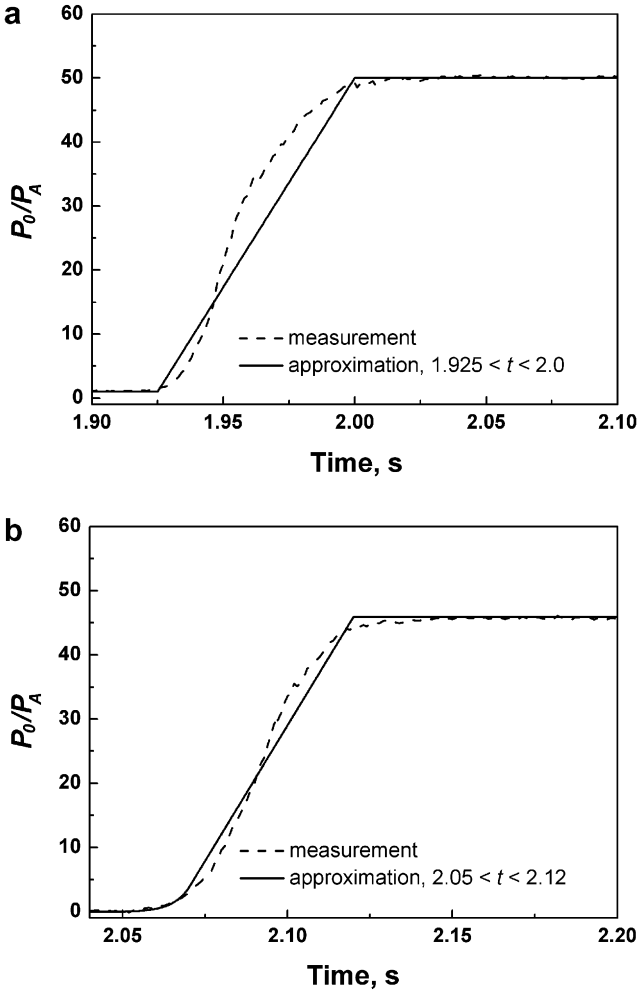

Fig. 8. Starting sequence of the opening valve and initialization of the nozzle inlet total pressure.

avoided, the diffuser wall should be protected by means of appropriate cooling methods such as water jacket or water spray. In this sense, a shorter diffuser is preferred owing to its lower thermal load and smaller construction budget. In addition, since a high-thrust rocket motor is generally tested in a vertical stand, it is all the more important to make the diffuser shorter. Thus, understanding the effects of diffuser length (L/D) on the steady performance and the starting characteristics of the SED is essential to its engineering application.

Taylor (1969) and Annamalai et al. (2000) have demonstrated in their experiments that there exists an optimum length-to-diameter ratio $(L/D)_{OPT}$ for diffuser starting. With the length-to-diameter ratio greater than or equal to $(L/D)_{OPT}$, the diffuser is always started with $P_{0,OPT}$. But the diffuser with the length-to-diameter ratio less than $(L/D)_{OPT}$ needs critical starting pressure higher than $P_{0,OPT}$. This critical starting criterium with regard to L/D is not theoretically predicted. For instance, a normal shock method, the simplest among relevant theories such as a normal shock theory (Annamalai et al., 1998), momentum theory (Foster, 1960), and Korst's theory (Korst, 1956), is unable to yield the correct $P_{0,OPT}$ for the starting locus of the short diffuser. One-dimensional shock configuration assumed in the theory conceptually replaces downstream shock-train with a single normal shock and thus geometrical parameters, such as diffuser length or shock-boundary layer interaction, are not taking into account as a factor affecting pressure recovery across the shock system. Consequently, previous researchers worked out

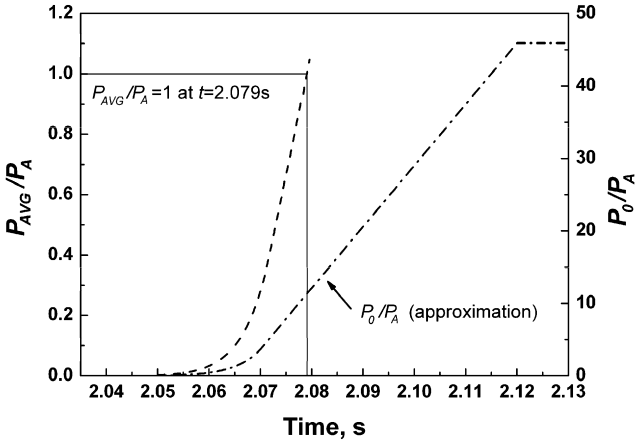

Fig. 9. Temporal change of pressure (P_{AVG}) averaged over the inner surface of the exit-cover. (When $P_{AVG} = P_A$, the exit-cover is removed numerically.)

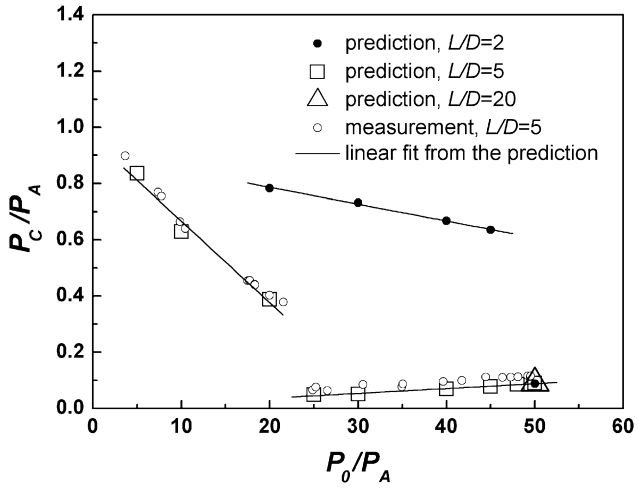

Fig. 10. Locus of starting and evacuation performance of straight cylindrical SED (L/D = 2, 5 and 20. Hysteresis occurring in a short diffuser operation was not considered).

a method in order for tuning $P_{0,OPT}$ for a short diffuser starting and proposed a correction factor (K-factor) which is defined as $(P_0/P_A)_{OPT,EXPERIMENTAL}/(P_0/P_A)_{OPT,THEORETICAL}$ and empirically determined. In spite of its practical significance, the reason why a shorter diffuser needs a greater $P_{0,OPT}$ for its starting than that of a longer diffuser has not been properly explained.

Since an upper-stage rocket motor is ignited in a low-pressure environment, high-altitude ignition test is another critical issue of HAT. Nevertheless, results of the ignition tests conducted at the low pressures are rare due to the difficulties in building up proper initial test-cell conditions. Propellant ignitability curves (Sutton and Biblarz, 2001) manifests that an ignition delay is shortened in proportion to an increase in the test-cell pressure, and this monotonic dependency is mainly due to the fact that the rate of chemical reaction and corresponding flame speed largely depend on an extent of the pressure. In the case of a low-pressure ignition test, the cell volume in the HAT which lacks in additional steam ejector system must be pre-evacuated. Keeping the diffuser exit capped with an exit-cover, a mechanical vacuum pump evacuates the vacuum chamber. After the rocket motor ignition, the SED starts and maintains the vacuum chamber pressure at a suitable level for successful HAT functioning. In addition to the aforementioned geometrical effects of shorter diffuser, the present study examines the evolutions of HAT starting and flow structures during initial stage of SED operation with pre-evacuation.

5.1. Effects of diffuser length on SED starting

Fig. 10 plots characteristic loci for a diffuser starting in terms of L/D (case 1 in Table 1). As illustrated in Fig. 2, the diffuser operation is characterized by two distinct operational modes: diffuser-unstarting and diffuser-starting modes. With P_0/P_A greater than $P_{0,OPT}/P_A$ ($P_{0,OPT}/P_A$ = 47.5 for L/D = 2; $P_{0,OPT}/P_A$ = 22.5 for L/D = 5), the diffuser is started. In contrast, an opposite holds when P_0/P_A is less than $P_{0,OPT}/P_A$. In the diffuser-unstarting mode, P_C decreases linearly in proportion to P_0 owing to an entrainment effect by high-speed nozzle exhaust. When the nozzle exhausts expands faster with higher dynamic pressure, the evacuation level (P_C) is lowered. This evacuation quality in the diffuser-unstarting mode cannot be theoretically quantified because the diffuser flows in this mode involve a variety of secondary flow phenomena such as movement of shock-induced separation and cascading shock wave structures. In Fig. 10, both the diffuser-starting and the diffuser-unstarting modes are correctly predicted and agreements are satisfactory at all driving pressures and diffuser lengths examined.

Mach number contour and streamlines of the shorter diffuser flows at an intermediate total pressure $P_{0,STD}/P_A$ of 40, (L/D = 2, middle of Fig. 11b) portray that expanding nozzle plume is detached and turns away from the diffuser wall. The vacuum chamber is not isolated and open to atmosphere with the presence of wall-recirculation flow. The diffuser is not started and serves as an internal passage for the nozzle plume only. In contrast, the flow

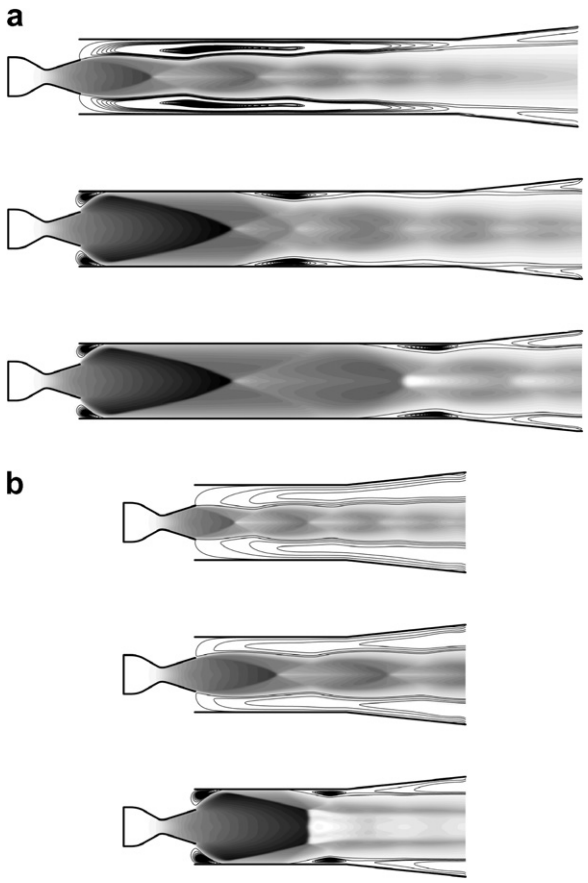

Fig. 11. Iso-Mach number and stream lines of steady diffuser flows at various driving pressures ($P_{0,STD}/P_A$) and diffuser lengths (L/D).

profile in the longer diffuser (L/D = 5, middle of Fig. 11a) exhibits complete diffuser starting and corresponding chamber evacuation. Higher P_0 above critical starting pressure is required to start the shorter diffuser. This distinct effect of L/D has been evidenced by numerous studies (Taylor, 1969; Annamalai et al., 2000) with regard to global performance parameters.

In a diffuser with $P_{0,STD}/P_A$ = 20 and L/D = 5 (top of Fig. 11a), recirculating flows are formed in the vicinity of diffuser wall and driven by highly-convective nozzle plume. However, for a shorter diffuser with $P_{0,STD}/P_A$ = 20 and L/D = 2 (top of Fig. 11b), streamlines between the diffuser wall and the nozzle plume show the presence of a reversed flow; flowing from the diffuser exit against the nozzle plume, reaching far upstream of the diffuser and turning back to the diffuser exit. The diffuser is not choked by the supersonic nozzle plume and the vacuum chamber is exposed to the potent influence of the atmosphere downstream. At the total pressures higher than an optimum starting pressure ($P_{0,OPT}$), expanding supersonic nozzle plume solidly touches down onto the diffuse inlet wall and isolates vacuum chamber by blocking the reversed flow from the atmosphere. The evacuation process becomes no longer affected by the atmosphere, and the chamber gas is drawn out by the nozzle exhaust of lower static pressure. This evacuation process continues until the chamber pressure is balanced to that of nozzle-exit. Regardless of L/D, the diffuser starting always causes a sudden drop of P_C/P_A in diffuser characteristic curve (Fig. 10) due to aforementioned shielding effect by supersonic flow at the diffuser inlet.

In the diffuser-starting mode, an axial position of the diffuser wall on which the nozzle exhaust impinges defines a location of the diffuser inlet. Mach number at the diffuser inlet (M_i) is invariant regardless of P_0 (in principle at least) as long as the diffuser choking is accomplished during the diffuser-starting mode. This hyperbolic nature is expressed by a simple function for the diffuser inlet pressure (P_i) linearly proportional to P_0 since, depending on one-dimensional isentropic-flow assumption, the ratio P_i/P_0 is only a function of M_i and invariant as well. Consequently, P_C which is balanced by the P_i in the diffuser-starting mode increases linearly with P_0 (Fig. 10).

A normal shock theory predicts theoretical optimum starting pressure ($P_{0,OPT}/P_A$) of the long diffuser (A_D/A_T = 28.4, L/D = 5) to be 20.6, but experimentally and numerically obtained value is commonly 22.5. Considerable amount of error in the theoretical prediction of $P_{0,OPT}/P_A$ occurs due to an application of the simple normal shock theory for a far different flow situation. The prediction error is not very large though, and less than 15% when the area ratio A_D/A_T is in the range of from 10 to 30 (Massier and Roschke, 1960; Annamalai et al., 2000). The diffuser with L/D = 5 is longer than its optimum and $P_{0,OPT}$ of 22.5 is higher than its minimum required for forming the normal shock. By contrast, the diffuser with L/D = 2 is too short to perform a successful starting because much higher $P_{0,OPT}$ of 47.5 is required. Evidently, the optimum L/D lies in between L/D = 2 and L/D = 5. It is also noticed from Fig. 12 that, at higher driving pressure of $P_{0,STD}/P_A$ = 50, the chamber pressures (P_C/P_A) obtained after starting the long diffusers (L/D = 5 and 20) yield almost same profiles of evacuation transients with same P_C converged. The short diffuser (L/D = 2) shows same evacuation performance (P_C/P_A) with the long diffusers once it is started. Aforementioned choking of the diffuser inlet by the supersonic flow enables the diffuser-starting. Once the diffusers are started, evacuation in terms of the chamber pressure (P_C/P_A) is unique regardless of the diffuser length.

Parametric analysis of diffuser starting due to different $P_{0,STD}$ and L/D is conducted. Initial cell pressure is assumed to be atmospheric (case 1 in Table 1). Fig. 12 shows pressure histories in the vacuum chamber in terms of L/D of 2, 5 and 20 when $P_{0,STD}$ is 25 and 50, respectively. In all calculations, time-marching was

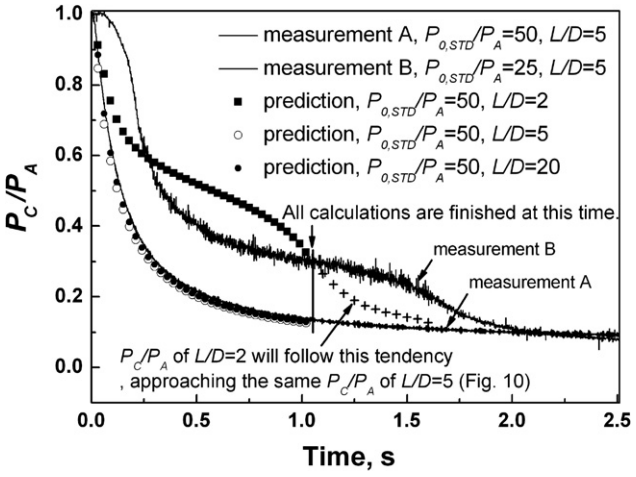

Fig. 12. Histories of chamber evacuation (P_C/P_A) during starting transient ($P_{0,STD}/P_A$ = 25 and 50, L/D = 2, 5 and 20).

stopped at an elapsed time of 1.1 s, and the chamber pressures due to the short diffuser (L/D = 2) after 1.1 s were interpolated with $P_{C,STD}/P_A$ = 0.09 from the diffuser characteristic curve in Fig. 10. Predictions for all cases of L/D of 5 and 20 when $P_{0,STD}$ is 50 show excellent agreements with measurements.

Plots in Fig. 12 exhibit two general characteristics featuring SED starting transients. On one hand, there is a threshold L/D over which the SED starting transient becomes unique. On the other hand, even with the same steady evacuation performance (P_C/P_A), the transient in diffuser mode-transition regime may not be unique. At same total pressure at nozzle inlet, the shorter diffuser (L/D = 2) exhibits vastly different initial transient. At higher driving pressure $P_{0,STD}/P_A$ of 50, the starting transient of the short diffuser (L/D = 2) contrasts with those of the long diffusers (L/D = 5 and 20). For the long diffusers, two declining pressure curves exhibit similar exponential decay. The chamber pressure due to the shorter diffuser is also decaying but its profile is neither exponential nor monotonic. Due to retardation of the jet impingement onto the diffuser inlet wall, a sudden drop of P_C/P_A occurs before the flow is stabilized to its steady state.

It was revealed from a series of starting test for a longer diffuser (L/D = 5) that an evacuation with non-exponential decay of P_C/P_A occurs when total pressure at nozzle inlet ($P_{0,STD}/P_A$) is slightly higher than an optimum starting pressure ($P_{0,OPT}/P_A$). Therefore, atmospheric starting of the straight cylindrical SED with a sudden drop of P_C/P_A can be characterized in terms of the driving pressure in the range between $P_{0,OPT}$ and P_0 slightly higher than $P_{0,OPT}$. For instance, two diffuser configurations; (1) $P_{0,STD}/P_A$ = 50 with L/D = 2 and (2) $P_{0,STD}/P_A$ = 25 with L/D = 5 lies in this regime, and the pressure records in the vacuum chamber exhibits a evacuation profile with a sudden drop of P_C/P_A (Fig. 12). It is noted that the non-exponential transition is not a function of diffuser length only and can occur at properly conditioned driving pressure. In the HAT of a short-duration engine, occurrence of this non-exponential decay is undesirable since it causes the problem of thrust distortion.

Annamalai et al. (1998) tested a model solid rocket motor in the HAT equipped with a straight cylindrical SED and reported an occurrence and duration of violent fluctuation of P_C/P_A in starting transient when P_0 is slightly lower than $P_{0,OPT}$. They addressed that the test nozzle may fail due to resonating vibration when the natural frequency of the test nozzle coincides with the frequency of the pressure fluctuation. However, in the present experiment, pressure fluctuation was not so violent at any driving pressures ($P_{0,STD}/P_A$) up to 20. In Fig. 12, pressure fluctuation becomes obvious from

the moment immediately before the nozzle-jet impingement (measurement B). But, this pressure fluctuation is not resonant, thus not amplified to drive hydraulic instability, and then attenuated to minimal after the diffuser is choked.

Fig. 13 shows snapshot contours of Mach number and streamlines evolving during the short diffuser starting ($L/D = 2$). As was visualized by Park et al. (2008), gas entrainment from the vacuum chamber is most active at the early stage of the starting transient and gets gradually weakened as the diffuser flow is stabilized into its steady state. A corner eddy at the diffuser inlet appears immediately after the formation of nozzle plume and gradually vanishes as time elapses (Fig. 13a–c). As the time passes over 50 ms, the nozzle plume is firmly formed and Mach disk originated at the diverging section of the nozzle moves downstream and disappears. Fig. 13 also shows the shock transition along the diffuser centerline: (1) from Mach to regular reflection between 5 ms and 50 ms and, successively; (2) from regular to Mach reflection between 100 ms and 1000 ms. In contrast to the results of long diffuser (Fig. 11a), a stronger local Mach disk is formed downstream of the shorter diffuser (Fig. 13f) because the flow passage is not long enough to build an appropriate shock structure through which the diffuser flows decelerate and adjust to the atmosphere smoothly.

Regardless of the diffuser lengths, general features of flow transitions reaching the diffuser starting are not distinctly different. However, as shown in Fig. 13e, a reversed wall-flow originating from the downstream atmosphere reaches far upstream before an impingement of the nozzle exhaust onto the diffuser inlet wall. If the driving pressure is not sufficiently high, expanding nozzle exhaust fails to impinge onto the diffuser wall and the diffuser is not started. In this situation, the supersonic jet from the nozzle stays in its form of nozzle plume with its pressure balanced with that of the reversed wall-flow as shown in Fig. 11b when $P_{0,STD}/P_A$ is 20 and 40. If P_0 is high enough to cause the impingement and solid starting of the diffuser, the nozzle exhaust blocks the reversed wall-flow and the flow separation point is shifted downstream (Fig. 13f). Considering the chamber pressures in Fig. 12 in view of the snapshot pictures in Fig. 13, aforementioned sudden drop of P_C/P_A occurs just ahead of the nozzle plume impingement.

For a long diffuser, diffuser choking is advanced by anchoring the sonic line on the diffuser inlet-wall before reversed wall-flow reaches the diffuser inlet. Detailed descriptions of this flow transition as well as the chamber gas entrainment during starting and terminating transients of the SED are provided in author's previous work (Park et al., 2008). In the case of the long diffusers, flow parameters of the nozzle exhaust need not be balanced with those of reversed wall-flow. Fig. 11a shows recirculation zone near diffuser inlet-wall driven by the nozzle exhaust. By contrast, the flow transition in the short diffuser is strongly affected by the reversed wall-flow and an optimum starting pressure of the short diffuser is higher than that of the long diffuser (Fig. 10). It is noted that an occurrence of the sudden drop of the vacuum chamber pressure peculiar in the short diffuser starting (Fig. 12) depends on the extent of the driving pressure, and thus is not observed in every starting transient.

5.2. Effects of initial cell pressures on SED starting

Fig. 14 depicts dynamic pressures measured in the vacuum chamber and at the diffuser exit wall when the SED is started from a pre-evacuated state (case 2 in Table 1). Initial vacuum pressure ($P_{C,INIT}/P_A$) in the cell volume (a volume inside the dotted line in Fig. 1) at the beginning (2.05 s) is 0.0027 which is low enough to mimic the high altitude condition. Immediately after opening the nozzle inlet value at 2.05 s, high-pressure nitrogen gas ($P_{0,STD}/P_A = 45.9$) charge the cell volume. This causes rapid cell pressurization since the diffuser exit is blocked off from the atmosphere by

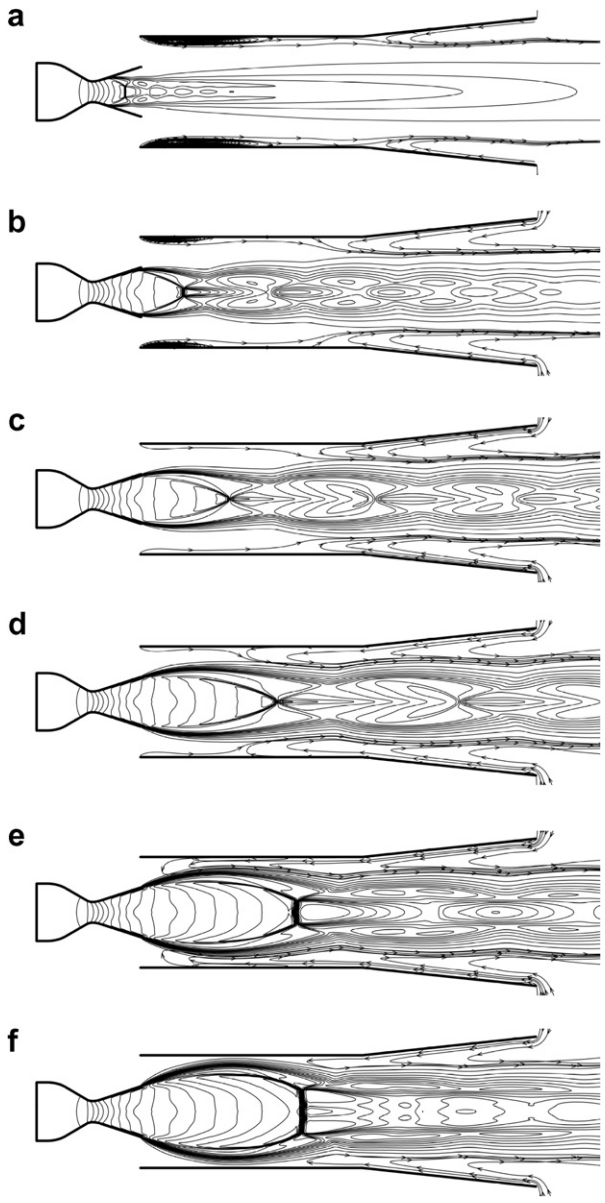

Fig. 13. Flows evolution during a short diffuser starting and instant profiles of Mach number contour and streamlines ($P_{0,STD}/P_A = 50$, $L/D = 2$, $t_0 = 1.925$ s).

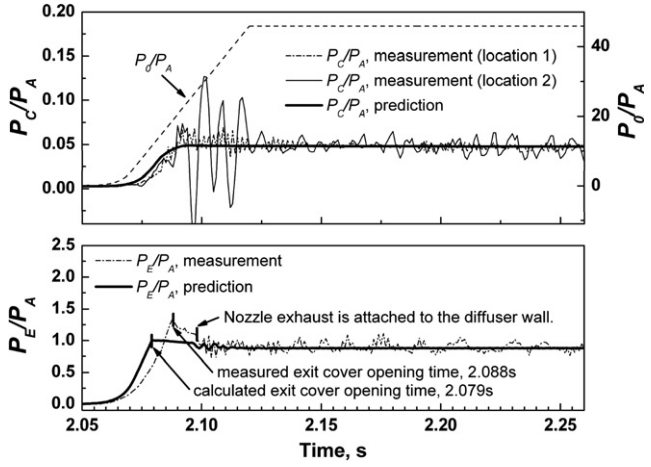

Fig. 14. Starting and steady-state pressures inside the vacuum chamber (upper) and at the nozzle exit wall (lower) with pre-evacuation (case 2).

the exit-cover (Fig. 1). The nozzle exhaust flows into the vacuum chamber of much lower initial pressure and increases the chamber pressure. With an increase in the driving and cell pressures, the pressure exerting on the inner surface of the exit-cover (P_{AVG}) also increases and exceeds an atmospheric pressure, and then the cover at the diffuser exit is lifted away and the nitrogen gas is discharged from the diffuser.

In Fig. 14, predicted P_E/P_A by and large deviates from the measurement in the early stage of operation, and the time and pressure for the exit-cover opening are underestimated. The exit-cover opening was experimentally recorded at 2.088 s and a little lagged from the prediction (2.079 s) and the opening pressure is higher than the atmospheric pressure. The prediction error is originated from: (1) inaccurate approximation of initial transient of P_0; (2) simple scenario of mechanical exit-cover opening. In Fig. 8b, a fitted line for P_0 overestimates the measurement in the interval between 2.05 s and 2.079 s. The faster cell-pressurization by this steeper increase in P_E/P_A results in an earlier opening of the exit-cover. In addition, depending on the scenario, the diffuser exit-cover is numerically removed at an instance when the pressure exerting on the inner surface of the exit-cover becomes atmospheric (Eq. (2)). Fig. 9 portrays this scenario with P_{AVG} and P_0 during the opening transient. But this scenario lacks in an additional force by the exit-cover. In the real situation, adhesive agent used to fix the exit-cover onto diffuser exit causes the peak of P_E/P_A higher than unity.

An instant profile of Mach number contour and streamlines immediately before the exit-cover opening ($t = 2.079$ s) is presented in Fig. 15. A large portion of the nozzle exhaust flows into the vacuum chamber and forms a supersonic flow region which prevails locally at vacuum chamber inlet. During the vacuum ignition test by the straight cylindrical SED with no use of the steam ejector system, occurrence of this plume blowback is unavoidable.

Fig. 16 shows evolution of the gas temperature immediately after exit-cover opening at 2.079 s. In contrast to over- to under-expansion transition in the case of atmospheric starting (Fig. 13), the nozzle exhaust in case 2 (Fig. 16) is always under-expanded due to lower cell pressure during the starting transient. Plume blowback is ceased immediately after the impingement of the nozzle exhaust onto the diffuser inlet-wall. The flow separation from the diffuser wall occurs and its location is shifted downstream paralleled with stabilizing vacuum-chamber pressure (Fig. 16d and e). Owing to this solid diffuser choking due to rapid nozzle exhaust expansion and blocking of the plume blowback, the pressure in the vacuum chamber is quickly lowered and equilibrated within 2.1 s (Fig. 14).

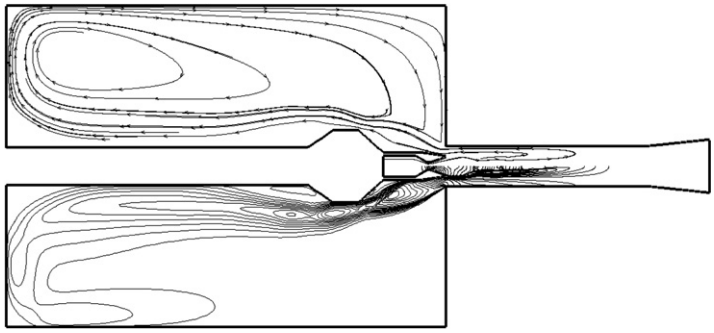

Fig. 15. Mach number contour (lower half) and streamlines (upper half) of the diffuser flow filling the pre-evacuated cell volume (case 2) at $t = 2.079$ s.

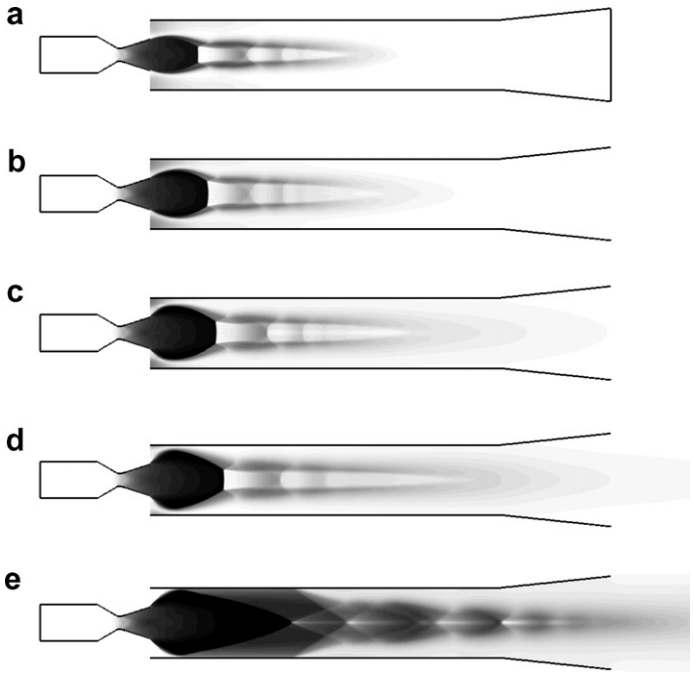

Fig. 16. Evolution of diffuser gas temperatures after exit-cover opening at t_0 ($t_0 = 2.079$ s).

After the formation of the diffuser flows in the diffuser starting mode, dynamic sensors recorded pressure fluctuations in the vacuum chamber and the diffuser downstream for a while. The pressure fluctuation induced by an abrupt blocking of mass inflows into the vacuum chamber is rapidly damped out as the pressures are equilibrated. On the contrary, the shock-boundary layer interaction at the diffuser downstream causes the pressure fluctuations, and this hydraulic instability, assisted by strongly convective diffuser flow, is sustained with finite amplitude. This highly time-dependent dispersive fluctuation is not captured in the present calculation since RANS method is unable to resolve the phenomena (Fig. 14). But, the prediction shows very good agreement with measured static pressures. Depending on their experimental results, researchers suggested that this type of shock oscillation is due to turbulent velocity fluctuations in the boundary layer upstream (Östlund, 2002). Also suggested is that changes in instantaneous turbulent velocity profile cause relocation of the shockwave and hence yield the unsteady shockwave oscillation.

6. Conclusions

Effects of diffuser length and pre-evacuation state on evolving diffuser flows in starting transient of straight cylindrical SED are numerically investigated. Preconditioned Favre-averaged Navier–Stokes in-house solver combined with a low Reynolds number k–ε model and Sakar's treatment for turbulence compressibility simulates internal and external diffuser flows. The numerical method is properly validated with accuracy. Parametric analysis of the SED suggests following conclusions.

1. Characteristic locus of diffuser-starting and diffuser-unstarting modes is constructed for the diffusers of three different lengths (L/D = 2, 5, and 20). Once the diffusers are started, steady evacuation performance in terms of vacuum-chamber pressure (P_C/P_A) is unique regardless of diffuser length. On the other hand, there exists a threshold L/D over which the SED starting transient becomes unique. The results for the diffuser mode-transition regime show that non-exponential variation of P_C/P_A prior to complete chamber evacuation largely depends on the diffuser length, but also can occur at a properly conditioned driving pressure.
2. Plume blowback into the vacuum chamber due to lower initial pressure ($P_{C,INIT}/P_A = 0.0027$) is observed. With no assistance by the separate gas (vapor) ejector system, an occurrence of this initial plume blowback is unavoidable, but it expedites expansion of nozzle exhaust and diffuser choking, and causes faster chamber evacuation than the atmospheric starting.

Acknowledgement

This work was supported by the Korea Research Foundation Grant funded by the Korean Government (MOEHRD, KRF-2006-511-D00085).

References

Annamalai, K., Visvanathan, K., Sriramulu, V., Bhaskaran, K.A., 1998. Evaluation of the performance of supersonic exhaust diffuser using scaled down models. Experimental Thermal and Fluid Science 17, 217–229.

Annamalai, K., Satyanarayana, T.N.V., Sriramulu, V., Bhaskaran, K.A., 2000. Development of design methods for short cylindrical supersonic exhaust diffuser. Experiments in Fluids 29, 305–308.

Bartosiewicz, Y., Aidoun, Z., Desevaux, P., Mercadier, Y., 2005. Numerical and experimental investigations on supersonic ejectors. International Journal of Heat and Fluid Flow 26, 56–70.

Desevaux, P., Lanzetta, F., 2004. Computational fluid dynamic modeling of pseudoshock inside a zero-secondary flow ejector. AIAA Journal 42 (7), 1480–1483.

Foster, R.M., 1960. The supersonic diffuser and its application to altitude testing of captive rocket engine. AFFTC-TR-60-1.

Hsieh, S.Y., Yang, V., 1997. A preconditioned flux-differencing scheme for chemically reacting flows at all Mach numbers. International Journal of Computational Fluid Dynamics 8.

Korst, H.H., 1956. Theory of base pressure in transonic and supersonic flows. Journal of Applied Mechanics 23, 593–600.

Massier, P.F., Roschke, E.J., 1960. Experimental investigation of exhaust diffusers for rocket engines. NASA CR 51076.

NASA Lewis Research Center, 1971. Captive-fired testing of solid rocket motors. NASA SPACE VEHICLE DESIGN CRITERIA, NASA SP-8041.

Östlund, J., 2002. Flow Processes in Rocket Engine Nozzles with Focus on Flow Separation and Side-Loads. Licentiate Thesis TRITA-MEK 2002:09, Department of Mechanics, Royal Institute of Technology, Stockholm, Sweden.

Park, B.H., Lim, J.H., Yoon, W., 2008. Fluid dynamics in starting and terminating transients of zero secondary flow ejector. International Journal of Heat and Fluid Flow 29 (1), 327–339.

Sankaran, S., Satyanarayana, T.V.V., Annamalai, K., Visvanathan, K., Babu, V., Sundararajan, T., 2002. CFD analysis for simulated altitude testing of rocket motors. Canadian Aeronautics and Space Journal 48 (2), 153–162.

Schäfer, K., Zimmermann, H., 2004. Simulation offlight conditions during lift off for rocket engine testing. In: AIAA/ASME/SAE/ASEE Joint Propulsion Conference, AIAA 2004-4001.

Shyy, W., Krishnamurty, V.S., 1997. Compressibility effects in modeling complex turbulence flows. Progress in Aerospace Sciences 33, 587–645.

Stephens, S.E., Bates, L.B., Lacasse, J.E., 1991. Geometry effects in second throat annular steam ejectors. In: AIAA/ASME/SAE/ASEE Joint Propulsion Conference, AIAA 91-2271.

Sun, D.W., Eames, I.W., 1995. Recent developments in the design theories and applications of ejectors – a review. Journal of the Institute of Energy 68, 65–79.

Sutton, G.P., Biblarz, O., 2001. Rocket Propulsion Elements, sixth ed. Wiley-Interscience. pp. 524–526.

Taylor, D., 1969. Ejector Design for a Variety of Application. AGARDograph #163.

Venkateswaran, S., Li, D., Merkle, C.L., 2003. Influence of stagnation region on preconditioned solutions at low speeds. In: 41st Aerospace Sciences Meeting and Exhibit, AIAA 2003-435.

Yang, Z., Shih, T.H., 1993. New time scale based model for near wall turbulence. AIAA Journal 31, 1191–1198.